HHS Public Access

Author manuscript

Int J Pharm. Author manuscript; available in PMC 2020 October 05.

Published in final edited form as:

Int J Pharm. 2019 October 05; 569: 118596. doi:10.1016/j.ijpharm.2019.118596.

Novel Olive Oil Phenolic (−)-Oleocanthal (+)-Xylitol-Based Solid Dispersion Formulations with Potent Oral Anti-Breast Cancer Activities

Mohammed H. Qusa[a], **Abu Bakar Siddique**[a], **Sami Nazzal**[b], **Khalid A. El Sayed**[a,*]

[a]School of Basic Pharmaceutical and Toxicological Sciences, College of Pharmacy, University of Louisiana at Monroe, 1800 Bienville Drive, Monroe, Louisiana 71201, United States.

[b]Department of Pharmaceutical Sciences, Texas Tech University Health Sciences Center School of Pharmacy, 5920 Forest Park Road, Dallas, Texas 75235, United States.

Abstract

Epidemiological studies have compellingly documented the ability of the Mediterranean diet rich in extra-virgin olive oil to reduce the incidence of certain malignancies, and cardiovascular diseases, and slow the Alzheimer's disease progression. *S*-(−)-Oleocanthal (OC) was identified as the most bioactive olive oil phenolics with documented anti-inflammatory, anticancer, and anti-Alzheimer's activities. OC consumption causes irritating sensation at the oropharynx via activation of TRPA1. Accordingly, a taste-masked formulation of OC is needed for its future use as a nutraceutical while maintaining its bioactivity and unique chemistry. Therefore, the goal of this study was to prepare a taste-masked OC solid formulation with improved dissolution and pharmacodynamic profiles, by using (+)-xylitol as an inert carrier. Xylitol was hypothesized to serve as an ideal vehicle for the preparation of OC solid dispersions due to its low melting point and sweetness. The optimized OC-(+)-xylitol solid dispersion was physically and chemically characterized and showed effective taste masking and enhanced dissolution properties. Furthermore, OC-(+)-xylitol solid dispersion maintained potent *in vivo* anti-breast cancer activity. It effectively suppressed the human triple negative breast cancer development, growth, and recurrence after primary tumor surgical excision in nude mice orthotopic xenograft models. Collectively, these results suggest the OC-(+)-xylitol solid dispersion formulation as a potential nutraceutical for effective control and prevention of human triple negative breast cancer.

Keywords

Extra-virgin olive oil; c-MET receptor tyrosine kinase; (−)-Oleocanthal; Solid dispersion; Taste masking; (+)-Xylitol

*Corresponding author at: School of Basic Pharmaceutical and Toxicological Sciences, College of Pharmacy, University of Louisiana at Monroe, 1800 Bienville Drive, Monroe, LA 71201, USA., elsayed@ulm.edu (K. El Sayed).

K. El Sayed is a Chief Scientific Officer in the Shreveport, Louisiana-based Oleolive without compensations. The rest of coauthors declare no competing financial interest.

1. INTRODUCTION

The extra-virgin olive oil (EVOO) phenolic secoiridoid (−)-oleocanthal (OC) is one of the most bioactive phenolics with documented anti-inflammatory and anti-bacterial activities (Pei et al., 2016; Segura and Curiel, 2018). It also possesses proven neuroprotective activities by enhancing the clearance of the Alzheimer's disease hallmark Aβ amyloid, and by protecting against H_2O_2-induced oxidative stress (Qusa et al., 2015; Batarseh et al., 2017; Giusti et al., 2018). In addition, OC was reported to control a wide range of cancer pathways including proliferation, migration, invasion, and angiogenesis among multiple cancer types (Akl et al., 2014; Cusimano et al., 2017). For instance, in breast cancer (BC), OC showed inhibitory activities of multiple molecular targets, such as the receptor tyrosine kinase (RTK) c-MET, mTOR, and STAT3 (Akl et al., 2014; Cusimano et al., 2017; Pei et al., 2016). OC also targeted the proteostasis key regulator chaperone machinery HSP90 and the estrogen receptor-α (ERα) (Akl et al., 2014; Ayoub et al., 2017).

Unfortunately, OC causes back of the throat (oropharynx) pungency and irritative sensation due to the activation of transient receptor potential cation channel subtype A1 (TRPA1) (Cicerale et al., 2009; Peyrot et al., 2011). Distinct nociceptors for OC are located in the oral cavity and the oropharyngeal region. However, OC irritation was not correlated with acid-induced irritation and hence OC was not exerting generalized acid-sensing irritation (Cicerale et al., 2009; Peyrot et al., 2011). OC irritating taste, high viscosity, solubility, reactive C-1 and C-3 aldehydes, and chemical instability significantly challenged the development of an acceptable oral formulation for human use. Therefore, the development of a novel taste-masked OC formulation that maintain its bioactivity, unique pharmacophoric features, stability, and enhance its water solubility would be a step-forward for its future clinical and functional food applications.

This study reports the characterization and biological testing of a novel (liquid)solid dispersion (SD) of OC. (Liquid)solid systems refer to formulations formed by the conversion of liquid active pharmaceutical ingredients (API) into dry powder using one of the SD methods (Vasconcelos et al., 2007). SD has been used to enhance the dissolution rate, solubility, oral absorption of poor water-soluble APIs and to mask their unacceptable taste (Vasconcelos et al., 2007; Sareen et al., 2012). SD formulations are prepared by blending a hydrophilic matrix and API; whereby the matrix can be either crystalline or amorphous solid while the drug is molecularly dispersed inside the inert carrier, creating a homogeneous glass solution (amorphous carrier) or solid solution (crystalline carrier) (Leuner and Dressman, 2000). Melting (fusion) and solvent evaporation methods are the two most frequently used SD preparation strategies (Tran et al., 2011). The melting method is appropriate for chemically stable and thermostable APIs (Medarevic et al., 2016). It includes melting an inert matrix (carrier) and/or API, followed by cooling, and mixing. This method is associated with high probability to change the formulated API and/or carrier properties (Baghel et al., 2016). One of the critical elements for successful SD formulation is the selection of appropriate carrier that should be compatible with the API.

Accumulating evidences show the ability of sweet and bitter taste compounds to share the same sensing sites at the human tongues. The capability of sweetening agents to trigger TRPA1 receptor suggests that sugar can play a critical role to mask the acrimony of OC (Lee and Owyang, 2017). The polyol sugar alcohols, represented by xylitol, sorbitol, and mannitol, are widely used excipients in pharmaceutical formulation that have been utilized as crystalline carriers in SDs. Polyols are commonly used in food industry due to their acceptable sweet taste, high solubility in water and non-carcinogenic effects (Asare-Addo et al., 2013; Lenhart and Chey, 2017; Shen et al., 2017). Xylitol is a polyhydric alcohol that has been classified as Generally Recognized as Safe (GRAS) additive by the US Food and Drug Administration (FDA) (Farah et al., 2011). It is used as sweeteners substitute in food due to its low glycemic index, high metabolic rate, and low toxicity margin (Chang et al., 2018; Jeon et al., 2012). Moreover, the unique refreshing and chilling sensations at the mouth distinguishes xylitol over other polyols for more effective taste masking (Sadler, 2014). Therefore, xylitol is viewed as an ideal excipient for use to enhance the dissolution and taste of APIs (Arafa et al., 2018). In this study, it was hypothesized that xylitol could be used as an appropriate carrier to prepare bioavailable (liquid) solid dispersion of OC with acceptable taste and dissolution profile for prospective future application as a nutraceutical (functional food). The optimized OC-xylitol SD thermodynamic complexation formulation (OC-X) was characterized physically by studying its crystal properties and chemically by spectroscopic methods. Finally, we verified the enhanced breast cancer preventive, growth, and recurrence inhibitory activity of OC-X formulation using orthotopic nude mouse xenograft model and identical experimental settings previously reported for plain non-formulated OC (Akl et al., 2014; Siddique et al., 2019`a`). Interestingly, plain non-formulated OC showed good activity in tumor growth suppression model but failed to prevent TNBC locoregional recurrence after primary tumor surgical excision unlike OC-X, which effectively prevented 60% of this aggressive tumor phenotype recurrence in identical model (Akl et al., 2014; Siddique et al., 2019`a`).

2. EXPERIMENTAL SECTION

2. 1. Chemicals and Reagents

All chemicals were purchased from VWR International (Suwanee, GA, USA), unless otherwise stated. *S*-(−)-Oleocanthal (OC) was extracted from EVOO (The Governor, Corfu, Greece) and its purity of >99% was established based on q^{1}H NMR analysis. (+)-Xylitol (99% purity, No. X00810) was purchased from Pflatz and Bauer (Waterbury, CT, USA). p-MET antibody was purchased from Cell Signaling Technology (Beverly, MA, USA). Water used throughout the study was double distilled. All other products and reagents were of analytical grade.

2.2. Preparation of solid dispersion (SDs)

SD formulations containing OC and (+)-xylitol were prepared using the hot melt fusion method (Kaialy et al., 2014; Maniruzzaman et al., 2013). (+)-Xylitol, mp 93–100 °C, a hydrophilic carrier, was melted by using IKA RCT basic hotplate at 100 °C, and OC (5 mg per batch) was then added. The molten mixture was quickly cooled by pouring into a non-sticky pan and subjected to N_2 flow for 5 min. Increasing ratios of OC-xylitol were

attempted started with 1:1 to 1:7, w/w, to reach acceptable solid batches as determined by full powder characterization. After solidification, samples were grinded, stabilized, and stored at room temperature in dark place for at least 24 h before analysis. A physical mixture (PM) of the OC and xylitol was made, by adding OC (5 mg per batch) directly to (+)-xylitol crystals with slow mixing of increasing ratios of xylitol starting with 1:1 to 1:7, w/w. Mixtures were then stored at room temperature in dark place for at least 24 h before analysis. Crystallized (+)-xylitol was prepared by melting the xylitol and then cooling under N_2 flow.

2.3. Scanning electron microscopy (SEM)

A Hitachi S-4800 Field-emission Scanning Electron Microscope (FE-SEM, Hitachi, Japan) equipped with liquid nitrogen-cooled sample preparation and Cryo-transfer units Gatan ALTO-2500 as cryo-preparation system. Scanning electron microscopy (SEM) was employed to examine the morphology of prepared SD and powder particles. To reduce specimen charging and thermal damage, samples were deposited on aluminum mounting pins at the specimen holder after adding carbon sticker then all specimens were gold coated (~5 nm thickness) using a Cressington Sputter Coater 208HR before imaging at 15.0KV accelerating voltage to make the final conduction on top of surface. Images of (+)-xylitol, crystallized (+)-xylitol, PM (1:7), and OC-X (1:7) SD were observed at an accelerating voltage of 3.0 kV at low detector, magnified at 30,000–50,000x and used 7.5–7.8 mm as a working distance. Macro-pictures were taken under microscope for each formulation. The same samples were also imaged under light microscope using 10x zoom.

2.4. Thermal analysis

Differential scanning calorimetry (DSC) measurements were performed on a TA 2920 modulated differential scanning calorimeter (MDSC, TA Instruments-Waters LLC., New Castle, DE). Accurately weighed samples of powdered (+)-xylitol, crystallized (+)-xylitol, OC-X SD and PM (1:7) were hermetically sealed in aluminum pans and empty pans were used as references. The specimens were equilibrated at 0 °C and then heated to 150 °C at a rate of 5 °C/min. Nitrogen gas was then purged through the DSC cell with a flow rate of 20 mL/min. Melting endotherms (Tm), endotherm full width at half maximum (FWHM), and enthalpy energy (ΔH) were generated using Universal Analysis 2000 version 4.2 software (TA Instruments Waters LLC, New Castle, DE). Thermogravimetric analysis (TGA) was performed for pure OC (5 mg) on a TA Q500 thermal analyzer at increasing heating rate of 5 °C min^{-1} from 5 to 800 °C under flowing N_2.

2.5. Powder X-ray diffraction (PXRD) analysis

Powder X-ray diffraction patterns were measured for (+)-xylitol, crystallized (+)-xylitol, OC-X SD, and PM (1:7) using a D8 DISCOVER X-ray diffractometer (Bruker Billerica, MA). PXRD measurement analysis was performed using Cu radiation, a voltage of 40 kV, and a current of 30 mA. The range (2ϕ) of scans was from 20° to 50°, which identifies all xylitol peak characteristics at a speed of 0.02° every second.

2.6. Molecular modeling study

Molecular modeling experiments were performed using Schrodinger molecular modeling software package installed on an iMac 27-inch Z0PG workstation with a 3.5 GHz Quad-core Intel Core i7, Turbo Boost up to 3.9 GHz, processor and 16 GB RAM (Apple, Cupertino, CA, USA). The monomeric structures of (+)-xylitol were constructed using the Glide module (v5.8, 2012, Schrödinger, New York, USA). Hydrogen bonding patterns were identified after energy minimizations at the molecular dynamic/solvent-free mode for (+)-xylitol and OC. OC-X SD H-bonding complexation was detected with up to 2 Å distance and optimal angle between 90–180° (Maniruzzaman et al., 2013).

2.7. Infrared (IR) analysis

FT-IR spectroscopic analysis was used to determine possible OC-xylitol complexation via SD and/or physical mixing. FT-IR spectra of OC, (+)-xylitol, SD OC-X and PM (1:7) were analyzed using a diffuse reflectance cell, without any prior sample preparation other than directly compressed on an ATR crystal under appropriate compression tip, acquired on a Perkin-Elmer Spectrum One FT-IR Spectrometer. All analyses recorded at 800–4000 cm^{-1}, with an average of 16 scans at 4 cm^{-1} resolutions.

2.8. Mass spectrometric (MS) analysis

Q1-MS and full product ion (PI) scanning experiments were conducted using an Applied Biosystems–MDS SCIEX API 3200TM triple quadrupole LC/MS/MS system (Applied Biosystems, Foster City, CA) equipped in a Turbo VTM Ion Spray TM source using MS with an electrospray ionization (ESI) interface operated in positive ion mode using Analyst version 1.4.1 software (MDS Sciex, Toronto). For MS, about 1 mg of dry physical mixture and SD OC-X were dissolved in 3 mL water and injected freshly within 1 min after dissolution. The MS system was optimized for Q1 at probe y-axis position 2 mm, probe X-axis position 5 mm, GS1 parameter controls the nebulizer gas 25 psi, curtain gas (CUR) 10 psi, declustering potential (DP) 35, entrance potential (EP) 10, desolvation temperature 550 °C. For PI, the MS was adjusted at low collision energy of 10V, which is less than the energy needed by OC to show its parent ions (18V) (Sanchez et al., 2017).

2.9. Dissolution studies

To assess the OC-X release changes, *in vitro* dissolution studies were performed for plain, non-formulated OC and its SD formulations using a USP type II dissolution apparatus (VK 7000, Varian Inc., Cary, NC) at a paddle speed of 100 rpm as previously reported (Hagbani and Nazzal, 2017; Cui et al., 2009). OC-xylitol concentrations of 1:7 and 1:70 were selected for dissolution study. The selection of 1:70 ratio was intended to: 1) compare the effect of higher xylitol concentration on OC dissolution, 2) mimic the potential for the use of larger amounts of xylitol in humans, and 3) consider the expected extensive xylitol gut microbiota metabolism (Uebanso et al., 2017; Tamura et al., 2013). Thus, plain OC (5 mg) and each of SD OC-X formulations 1:7 and 1:70 were placed in hydroxypropyl methylcellulose (HPMC) capsules size-1 and used for dissolution experiments. Each sample capsule was dropped into a dissolution vessel containing 50 mL of SS 5 simulated saliva, pH 6.8, dissolution media and maintained at 37±0.5 °C (Marques et al., 2011). Capsules were held at the bottom of the

vessels using sinkers. Samples (2 mL) were withdrawn at predetermined time intervals, filtered, and analyzed spectrophotometrically at 340 nm. Each sample withdrawn was replaced with another 2 mL fresh dissolution medium.

2.10. Taste-masking assays (E-Tongue test)

The taste-masking assays were conducted on Alpha MOS ASTREE E-Tongue system equipped with an Alpha MOS pharmaceutical analysis sensor set #2 composed of seven liquid cross-selective sensors (ZZ, AB, GA, BB, CA, DA, and JE) (Wei et al., 2015; Podrazka et al., 2018). A 48-positions auto sampler and 25 mL-beakers were used for sampling and the acquisition times were fixed at 120 sec. Data generated by ASTREE system processed using multidimensional statistics-Alpha Soft v15.0 software (Wei et al., 2015; Podrazka et al., 2018). Taste analysis was conducted in artificial saliva (SS 5), pH 6.8 without enzymes (Marques et al., 2011); X1, used as a vehicle control, non-formulated OC; X2, SD OC-X formulations 1:7 and 1:70 w/w; X3 and X4, respectively, and placebo (+)-xylitol; X5. To avoid cross sample contaminations, three successive deionized water cleaning runs were conducted between each sample. The Euclidian distances between formulations were calculated by the Alpha MOS ASTREE E-Tongue to assess the taste proximity between samples. The lower the distance, the closer the taste. Discrimination index (DI in %) was determined for each formulation and placebo pair. The closer the DI to 100%, the greater the distance between the centers of gravity, and the smaller the dispersion within groups.

2.11. Animal studies

The effects of SD OC-X 1:7 formulation administration against the development, growth and recurrence of the human triple negative breast cancer (TNBC) MDA-MB-231 cells orthotopically xenografted in nude mice were assessed. Foxn1^{nu}/Foxn1^{+}, 4–5 weeks old, female athymic nude mice were purchased from Envigo (Indianapolis, IN, USA). All animal experiments were approved by the Institutional Animal Care and Use Committee (IACUC), University of Louisiana at Monroe, protocol number 18 MAY-KES-03, with good animal practice defined by the NIH guidelines (National Research Council, 2011). Mice were acclimated to University of Louisiana-Monroe College of Pharmacy animal housing facility and maintained under clean room conditions in sterile filter top cages using ALPHA-Dri bedding and high efficiency particulate air-filtered ventilated racks at 25 °C, 55–65% relative humidity, and 12 h light/dark cycle for a week before experiments. Mice had free access to drinking purified water and pelleted rodent chow (no. 7012, Envigo/Teklad, Madison, WI).

2.11.1 Culture of MDA-MB-231 cells—MDA-MB-231 cells were purchased from ATCC (Manassas, VA). Cells were cultured in RPMI-1640 supplemented with 10% fetal bovine serum (FBS), 100 U/mL penicillin G, 100 μg/mL streptomycin,2 mmol/L glutamines and 100 μg/mL sodium pyruvate 100 mM. Cells were incubated at 37 °C in a humidified 5% CO_2 incubator until reach for 90 % confluence.

2.11.2. Tumor xenograft studies—Xenograft procedures were performed as previously described (Akl et al., 2014; Ayoub et al., 2017; Siddique et al., 2019`a–c`).

Briefly, mice were subcutaneously inoculated MDA-MB-231/GFP human breast cancer cells (1×10^6 cells/30 μL) in both recurrence and development modes and 2×10^6 cells/30 μL in growth mode. OC-X SD formulation 1:7 was used in all experiments at a daily dose of 10 mg/kg, the standard oral OC dose that showed excellent pharmacodynamic effects in different BC mouse models (Ayoub et al., 2017; Siddique et al., 2019`a–c`). During initial experiments, mice treated with oral xylitol encountered notable hypoglycemia due to elevating fatty acid oxidation-related genes in animal livers (Amo et al., 2011; Kovalkovicova et al., 2009). To avoid this limitation, especially with extended OC-X dosing, equivalent sucrose amount was added to each OC-X oral dose. This effect is observed only in mice, rats, and dogs but not in humans (Amo et al., 2011; Kovalkovicova et al., 2009). OC-X doses were freshly reconstituted in purified water just before dosing. Progressing animal tumors were monitored every other day. Tumor volume (V) was deduced by: $V = L/2 \times W^2$, where L is length and W is tumor width. Mice body weight and general health signs including food and water consumption, defecation, urination, and physical activity were carefully monitored daily.

Prevention mode.: Mice were randomized into two groups: (1) placebo-treated control group with xylitol and sucrose (n = 5); and (2) OC-X 1:7 SD formulation-treated group (n = 5). Treatment started 45 days before tumor cells inoculation and continued for additional 25 days. All mice were sacrificed on the 70th experiment day, and individual tumors were excised and weighed.

Growth mode.: Five days post-inoculation, animals developed tumors and were randomized into two groups: (1) placebo-treated control group with xylitol and sucrose (n = 4); and (2) OC-X 1:7 SD formulation and sucrose-treated group (n = 4). Oral daily treatments started on the 5th day post-inoculation of tumor cells for 15 days. All mice were sacrificed on the 20th day post-inoculation, and individual tumors were excised and weighed.

Recurrence mode.: Tumor cells inoculated on day-1 and on the 15th day post-inoculation, tumors then became palpable and reached average volume of 400 mm^3. Mice were then anesthetized using xylazine and ketamine (Akl et al., 2014; Ayoub et al., 2017), the primary tumors were surgically excised, and the wound was stitched under sterile conditions. One day after the surgery, mice were randomized into two groups: (1) placebo-treated group + sucrose (n = 5); and (2) OC-X + sucrose-treated group (n = 5) and oral treatments started and continued daily for 30 days. All mice were then sacrificed, and individual tumors were excised, collected, and weighed.

2.12. Statistics

Data analysis was performed using GraphPad Prism software version 8.1.0. (La Jolla, CA, USA). The results are presented as mean ± standard error of the mean (S.E.M.) for continuous variables. Differences among various treatment and control groups in animal study were determined by the paired *t*-test, Statistical comparison of means within different groups in the other experiments were investigated with two-way analysis of variance (ANOVA). p Values of <0.05 were considered to be statistically significant.

3. RESULTS

3.1. SEM imaging

The micro and macrostructural surface morphological features of (+)-xylitol, crystallized (+)-xylitol, PM (1:7), and OC-X (1:7) SD formulations were characterized by SEM (Fig. 1). The micro structure of the (+)-xylitol showed as subangular subrounded particles with smooth surfaces containing fine particulates and smoothly curved sides (Fig. 1A). The hot melt fusion process significantly affected the shape and surface morphology of xylitol particles in crystallized (+)-xylitol, showing more fine particles (Fig. 1B). OC-xylitol PM showed the entry of oily OC globules within the xylitol particles at the surface and agglomerates with xylitol to build clumps with smooth surface (Fig. 1C). OC-X SD formulation demonstrated a rough (wrinkled) surface texture in which OC competed with xylitol during the layer-by-layer formation process, resulting in heterogeneous OC and xylitol distribution within the crystallization matrix (Figs. 1D and S1).

3.2. Thermal analysis

Representative endotherm properties of unmodified (+)-xylitol, crystallized (+)-xylitol, OC-X SD and PM were acquired and compared (Fig. 2A). Melting point (Tm), endotherm full width at half-maximum (FWHM) and enthalpy energy (ΔH) were determined based on modulated temperature DSC (MTDSC) curves (Table 1). DSC results exhibited a characteristic melting peak at 95.65 °C and 95.46 °C for the (+)-xylitol and PM, respectively, which was consistent with literature (Fig. 2A) (Kuno et al., 2005). Moreover, DSC analysis showed that physically loading OC on xylitol caused reduction in the enthalpy energy (ΔH) of (+)-xylitol from 196.5 J g^{-1} to 187.3 J g^{-1}. Meanwhile, crystalized (+)-xylitol enhanced the ΔH by about 29.3 J over the non-crystallized (+)-xylitol (225.8 J g^{-1} versus 196.5 J g^{-1} for crystallized and (+)-xylitol, respectively) with the same melting peak at 95.25 °C and full width at half-maximum (FWHM) of 6.6 °C. Likewise, dispersion of xylitol with OC induced a thermodynamic complexation reaction, which resulted in the reduction of the melting peak and enthalpy energy to 94.11 °C and 211.7 J g^{-1}, respectively. However, FWHM remained the same; 6.95 °C, compared to crystalized (+)-xylitol. Further zoom at the (+)-xylitol melting point showed the presence of sharp diffraction angles with no halo background or peak widening, confirming the crystalline nature of all samples. The absence of the monoclinic hygroscopic metastable form of xylitol samples was indicated by lacking the endothermic transitions around 61 °C (Kaialy et al., 2014). The thermogravimetric (TG) analysis of pure non-formulated oily OC showed a minor mass reduction of 3% starting at 20 °C till 100 °C, which could be due to thermal evalporation of the adsorbed water in OC sample (Fig. 2B). Furthermore, OC thermogram also showed maximum decomposition in a two-step process, the major one started at 250 °C to 400 °C (mass loss of 63.45%) and the OC complete degradation was observed at 600 °C (Fig. 2B).

3.3. Powder X-ray diffraction (PXRD)

PXRD was used to determine phase purity and phase transformation. The diffraction patterns of the crystalized (+)-xylitol identified new characteristic peaks with higher intensity than the xylitol peaks, considering the formation of hard-out layer on the xylitol particles after applying melting SD method which confirms that melting process changed the

morphology of the xylitol crystal (Fig. 3). PM showed different peak position and intensity, suggesting that OC oily layer accumulated at the surface of the crystal could cause X-ray scattering at a different angle, compared to (+)-xylitol and crystallized (+)-xylitol. Similarly, PXRD pattern of OC-X SD formulation presented identical peak positions but with lower intensities, compared to PM.

3.4. Molecular modeling

To understand possible intermolecular interactions between OC and (+)-xylitol in the SD formulation, an *in-silico* interaction study in solvent free condition was performed. Both xylitol and OC structures sketched on the Maestro 9.3 panel interface (Maestro, version 9.3, 2012, Schrödinger, USA). Lig Prep 2.3 module (Lig Prep, version 2.3, 2012, Schrödinger, USA) was used to generate the 3D structures and to search different conformers. The OPLS (OPLS_2005, Schrödinger, USA) force field was applied to geometrically optimize each structure and to compute partial atomic charges. Thirty-two poses per structure were generated with different steric features for subsequent docking study using the Glide 5.8 module (Glide, version 5.8, 2012, Schrödinger, USA) in extra-precision (XP) mode. Initially, the intermolecular interaction between two xylitol molecules A and B was studied (Fig. 4A). Two hydrogen bonding patterns were identified and in the (+)-xylitol crystal (Fig. 4A). Xylitol molecule A showed hydrogen bond donating interaction between its C-1 OH group oxygen with the C-4 OH of xylitol molecule B (Fig. 4A). Meanwhile the C-4 OH of xylitol molecule A accepted hydrogen bond interaction with the C-1 of xylitol molecule B. This was encouraged by the proximity of these functional groups through space, 1.89 Å and 1.91 Å, respectively, along with their hydrogen bonding interaction angles, 173.9° and 167.6°, respectively. When xylitol and OC docked together, OC was able to mimic the 3D-orientation of xylitol and also contributed hydrogen bonding interactions with the xylitol C-1 OH oxygen accepting hydrogen bond interaction with the OC C-6’ phenolic hydroxyl group while the xylitol C-4 OH donated a hydrogen bond interaction with OC C-3 aldehyde oxygen (Fig. 4B). The thru-space proximity and interaction angles of xylitol-OC hydrogen bond interacting functionalities were very close to those of xylitol-xylitol interactions (1.86 Å, 168.8° and 1.86 Å, 150.8°, respectively, Fig. 4B). This clearly highlighted the potential of xylitol-OC electrostatic interactions through proximity 3D-alignments of their interactive functional groups.

3.5. IR analysis

The FT-IR spectra of placebo (+)-xylitol, non-formulated OC, OC-X 1:7 SD, and PM were compared (Fig. 5). The most characteristic peaks for OC are those at 1680 and 1723 cm^{-1} (C-1 and C-3 CHO aldehydes stretching, respectively) and the aliphatic CH stretching vibration sharp peak at 2726 cm^{-1}. These unique OC peaks were clearly displayed in both OC-X and PM (Fig. 5). An intense broad band at 3409 cm^{-1} corresponding to the OC free phenolic OH stretching vibration was evident in non-formulated OC but was overlapping xylitol OH stretching peaks (3361 cm^{-1}) in PM and OC-X. OC-X SD formulation showed a slightly shifted OH broad band (3390 cm^{-1}), which may be justified by possible intermolecular hydrogen bonding between OC and xylitol. Comparison of the fingerprint region provides diagnostic information for the identity and characteristic functional groups (Alkhamis et al., 2002; Fujimoto et al., 2016; Madgulkar et al., 2016). A strong OC-derived

band at 920 cm^{-1} was missing in the OC-X SD formulation but was evident in the non-formulated OC and PM (Fig. 5). Another xylitol-derived band at 1135 cm^{-1} was also missing in the OC-X formulation but was evident in the IR spectra of the placebo (+)-xylitol and the PM (Fig. 5). This further suggest potential involvement of OC and (+)-xylitol of the OC-X SD formulation in chemical complexation that masked some of the characteristic IR fingerprint bands.

3.6. Mass Spectrometric (MS) Analysis

MS analysis of non-formulated OC, (+)-xylitol, PM, and OC-X was performed in positive ion quadrupole mass analyzer (Q1) mode. MS data of PM (Fig. 6A) and OC-X (Fig. 6B) identified the precursor ion peaks of xylitol at *m/z* 175.1 $[M+Na]^+$, 153.7 $[M+H]^+$, along with its fragment at *m/z* 135.4 $[M-OH]^+$ (Figs. 6A and 6B). MS data of OC-X and PM also identified the precursor ion peaks of OC at 327.6 $[M+Na]^+$, 304.9 $[M+H]^+$, along with its monohydrate at *m/z* 345.6 $[M+Na]^+$ and the OC diagnostic fragment at *m/z* 121.4 (4-ethylphenol), which was consistent with literature (Figs. 6A and 6B) (Sanchez et al., 2017). MS spectrum of OC-X (Fig. 6B) also showed a new significant peak at *m/z* = 479.8, representing the OC-xylitol thermodynamic complexation peak $[OC+xylitol+Na]^+$. This peak disappeared after approximately 5 minutes of dissolution in water at room temperature. When OC-X has been subjected to high fragmentation energy (10v) at product ion mode (Fig. 6C), the intensity of the OC main peak at *m/z* 327.1 $[M+Na]^+$ and xylitol peak *m/z* 175.1 $[M+Na]^+$ significantly increased with notable diminishment of the characteristic peak at *m/z* 479.8 $[OC+xylitol+Na]^+$, suggesting possible reversible thermodynamic complexation between OC and (+)-xylitol under SD condition.

3.7. Dissolution

Plain non-formulated OC dissolution rate was compared with OC-X 1:7 and OC-X 1:70 SD formulations (Fig. 7). The cumulative dissolved OC concentration, based on analytical HPLC, was 60% for OC-X 1:7 after 10 minutes. Plain OC and OC-X 1:70 dissolved OC amount at the same point was 38% and 35%, respectively. Interestingly, after 15 minutes there was a dramatic upsurge in OC dissolution in OC-X 70X SD that reached 75% but OC-X 1:7 was still better in OC dissolution showing 80% OC dissolution at the same time point. Plain OC showed 57% OC dissolution at the 15 minutes point. Dissolution results after 40 minutes indicate that 100% of OC dissolved in both OC-X SD formulations while the plain OC needed more than 60 minutes for complete dissolution (Fig. 7).

3.8. Taste masking

The comparative percentage between two principal component analyses (PCA1-PCA2) were used to describe the total variation of the data by converting the data acquired by the E-tongue from seven different taste sensors to two-dimensional data (Wei et al., 2015; Podrazka et al., 2018; Dyminski et al., 2006; Ciosek and Wroblewski, 2007; Kobayashi et al., 2010; Legin et al., 2003; Zhang et al., 2015; Woertz et al., 2011). The system was able to clearly discriminate the taste map analysis between the vehicle control artificial saliva (X1) and the plain non-formulated OC (X2) (Fig. 8A). Moreover, the distances between the OC-X 1:7 (X3) and 1:70 (X4) SD formulas was much closer to the placebo xylitol (X5) and far from the plain OC (X2), which considered as the bitterest sample. The Euclidian distances

and percentage DI between samples were calculated to assess taste proximity; the lower the distance, the closer the taste. Fig. 8B shows an expected large distance between the vehicle control (X1) and the plain OC (X2, distance 143, DI 84%). Interestingly, the placebo xylitol (X5) was close to respective active formulas OC-X 1:7 (X3) and OC-X 1:70 (X4) by xylitol concentration-dependent distances; 60 and 29, respectively (Fig. 8B). The DI between X3 and X5 was 42 while the DI between X4 and X5 was 15, suggesting very close taste similarity to the plain non-medicated xylitol and confirming efficient OC taste masking.

3.9. *In vivo* anti-breast cancer activities

The *in vivo* activity of OC against BC has been previously demonstrated through targeting c-MET RTK and its downstream pathways (Akl et al., 2014; Ayoub et al., 2017; Siddique et al., 2019`a–c`). This study evaluated the *in vivo* anti-TNBC activity of OC-X 1:7 SD formulation in athymic nude mouse model orthotopically xenograft MDA-MB-231 cells. Testing used three different modes: preventive, growth, and recurrence (Fig. 9). In the preventive mode, administration of OC-X for 45 days before xenografting delayed the latency of tumor for two days, with overall tumor growth inhibitory rates of 49%, compared to placebo-treated control group (Fig. 10A).

In the growth mode, 15-day OC-X oral use suppressed TNBC growth by 48% compared to the placebo control group (Fig. 10B). In the recurrence mode, OC-X treatment extended the recurrence-free survival by two days compared to placebo control treated group. Furthermore, in placebo control-treated group, all 5 mice developed recurred tumors (100% recurrence rate) unlike the OC-X-treated group in which only 2 out of 5 mice recurred tumors (40% recurrence rate) (Figs. 10C and S2). OC-X treatment also significantly reduced the recurrence tumor volume compared to the placebo treatment (Fig. 10D, Siddique et al., 2019`a`). Due to the significant growth of the recurrent tumors in one placebo control and one OC-treated mice, both mice were sacrificed on the 24th day after surgery. This was reflected in both Figs. 10C and 10D. Over all *in vivo* experiment courses, no adverse effects, clinical changes, nor body weight reduction observed in treated mice (Fig. S3, Siddique et al., 2019`a`). Western blotting examination of the growth mode tumors collected after animals sacrificed showed a marked reduction (76%) in the intratumoral level of phospho-c-MET (Y1234/1235) compared to the placebo-treated control group tumors (Fig. 10E).

4. DISCUSSION

(−)-Oleocanthal is a unique bioactive natural product lead exclusively occurring in EVOO with well-documented beneficial activities against cancer, inflammatory and Alzheimer's diseases. OC consumption causes irritative sensation at the oropharynx cavity due to the activation of transient receptor potential cation channel subfamily A, member 1 (TRPA1) receptors. Accordingly, a taste-masked formulation of OC is needed for its future therapeutic use as a nutraceutical. This formulation should also consider the unique pharmacophoric features of OC, including the two highly reactive aldehyde groups, ester, and phenolic functionalities. Specifically, the OC reactive C-3 aldehyde tends to form hydrate (gem-diol) in water imparting amphiphilic characters (Sanchez et al., 2017; Siddique et al., 2019`c`).

The hot melt (fusion) solid dispersion method was selected in this study to formulate OC, an oil compound, as a (liquid) solid system. This was particularly important because methanol, ethanol, and water will chemically acetalize OC C-1 and C-3 aldehydes causing instability and undesired pharmacophoric changes. The GRAS ranked FDA-approved food additive (+)-xylitol was precisely selected based on cooling sensation inside the mouth, low melting point (below 100 °C), water solubility, thermal stability, low glycemic index, high metabolic rate, low toxicity, and initial effective OC release from its xylitol SD formulation (Chang et al., 2018; Jeon et al., 2012; Arafa et al., 2018; Kaialy et al., 2014; Milgrom et al., 2009`a`; Milgrom et al., 2009`b`. Mixing OC with melting xylitol and then cooling until the xylitol becomes fully crystallized afforded OC-X, a unique SD formulation that was physically and chemically different from simple physical mixing. This was confirmed and characterized by using different microscopic and spectroscopic methods. OC-X 1:7 was an optimal ratio affording good flowability, hardness, and surface roughness while at the same PM ratio has paste, semisolid-like appearance. Further physical characterization of OC-X 1:7 by DSC and PXRD confirmed different physical properties compared to PM. OC PM loading decreased the enthalpy energy of xylitol, which indicated that OC can enhance the thermal energy transfer between xylitol particles. Yet, xylitol melting peak was shifted in the OC-X SD due to thermodynamic complexation of OC and xylitol via hydrogen bonding interactions. Recrystallization of xylitol to more stable form with harder out layer compared to the original crystalline xylitol enhanced its enthalpy energy. The similarity of FWHM for all samples implied disordered OC distribution inside the xylitol matrix.

TGA and DSC suggest that the change in OC-X as it compared to individual formulation ingredients and PM is beyond the physical morphology change. The lack of significant OC weight loss at the xylitol melting point in TGA confirmed the appropriate OC thermal stability to use the SD method with xylitol carrier. Furthermore, PXRD results showed the heterogeneous nucleation of xylitol in OC-X SD formulation in which OC settled inside the xylitol matrix and not on surface, which provided appropriate environment for thermodynamic complexation. Interestingly, molecular modeling study in a solvent-free condition suggested the potential of OC to adapt a 3D confirmation that will encourage two hydrogen bond interactions with xylitol, which was parallel to those of interactions of two xylitol molecules with each other. Spectroscopic characterization of OC-X using FTIR and ESI-MS confirmed the novel thermodynamic complexation of OC with xylitol. OC-X showed new fingerprint region peaks in the FTIR and a new molecular ion peak *m/z* at 479.8, representing the sodium adduct of OC-xylitol thermodynamic complexation peak $[OC+xylitol+Na]^+$. This later peak was MS-MS fragmented at low fragmentation energy to OC *m/z* 327.1, $[M+Na]^+$ and xylitol *m/z* 175.1, $[M+Na]^+$, confirming their complexation. This peak disappeared within 5 minutes after dissolution in water due to possible rapid OC-xylitol thermodynamic complex dissociation. The IR and ESI-MS findings for OC-X were not observed for PM.

The dissolution rate is proportional to the surface area (Zhang et al., 2018). Reducing OC particle size is expected to enhance its dispersibility inside the (+)-xylitol matrix and subsequent water solubility unlike the plain non-formulated OC, which tends to aggregate and builds a single oil cluster layer. Dissolution studies indicated that OC-xylitol 1:7 was better than 1:70 in enhancing dissolution, especially at the first 15 min. The OC-X 1:7

formulation needed 40 min for complete dissolution in water, unlike the plain OC, which needed more than 60 min using a USP type II dissolution system. This confirmed the superior dispersion of OC-X versus plain OC.

OC taste masking will facilitate its use as future nutraceutical and food additive. No previous attempt in literature dedicated to mask the OC taste for oral delivery. The E-Tongue experiment showed the effective ability of (+)-xylitol to mask the irritative OC taste. The higher the xylitol amount, the more effective the taste masking. The potential OC-xylitol complexation in addition to the unique cooling sensation taste induced by xylitol may have contributed to the effective taste masking.

The *in vivo* anti-BC activity of OC is well documented and mostly through targeting the c-MET RTK and its downstream pathways including mTOR, Akt, STAT3, ERK½, MAPK, and HSP90 (Pei et al., 2016; Akl et al., 2014; Ayoub et al., 2017; Siddique et al., 2019`a–c`). Dysregulation of c-MET correlates with aggressive proliferation, invasive, and pathological motility profiles in breast and several other cancers (Akl et al., 2014; Ho et al., 2015). c-MET amplification also correlates with the escape of cancer cells from anticancer effects of several targeted therapies (Akl et al., 2014; Siddique et al., 2019`b`; Ho et al., 2015). The essential role of c-MET pathway in human BC, specifically TNBC, development and recurrence is well documented (Ho et al., 2014; Samiee et al., 2012; Pienta et al., 2013; Comen et al., 2011). Residual surviving cancer cells can also repopulate tumors after excision surgery, radiation therapy, or during chemotherapy cycle gap periods (Ho et al., 2014; Samiee et al., 2012; Pienta et al., 2013; Comen et al., 2011). c-MET dysregulation can trigger activation mechanisms of dormant tumor cells, triggering repopulation and subsequent relapse and recurrence (Ho et al., 2015; Ho et al., 2014; Samiee et al., 2012; Pienta et al., 2013; Comen et al., 2011). The c-MET modulator micronutrient OC can prevent or delay BC development, suppress and abrogate its progression and recurrence. The high daily dietary EVOO consumption is common in the Mediterranean populations, with documented epidemiological studies showing less incidence of breast and colon cancers versus western populations (Toledo et al., 2015; Escricha et al., 2011).

OC-X showed potent oral anti-TNBC activities in orthotopic nude mice xenografts. In early treatment-preventive mode, OC-X extended the tumor-free survival by two days and potently suppressed the developed tumor growth. OC-X also showed potent tumor growth suppression when used after tumor cells xenografting. Interestingly, OC-X prevented 60% of TNBC recurrence after primary tumor surgical excision in nude mouse xenograft model. Only 2 out of 5 mice had locoregional recurrent TNBC compared to 5 out of 5 mice in placebo-treated group. Recently, in an identical model, plain non-formulated OC was not able to prevent TNBC recurrence and therefore 5 out of 5 nude mice treated with plain OC developed locoregional recurrence tumors (Siddique et al., 2019`a`). Plain OC was only able to delay and suppress the locoregional recurred TNBC MDA-MB-231 cells tumor volume (Siddique et al., 2019`a`). This clearly shows the improved pharmacodynamics conveyed by the use of OC-X SD formulation as compared to the non-formulated OC. Analysis of tumor lysates treated with OC-X showed effective suppression of c-MET activation suggesting successful maintenance of OC previously reported anti-BC effects at the molecular level (Akl et al., 2014; Siddique et al., 2019`a–c`).

5. CONCLUSION

Oleocanthal is an exceptional natural product exclusively occurring in EVOO and has documented activities against cancer, inflammatory conditions, and Alzheimer's disease. The present study developed a novel xylitol-based liquisolid SD formulation with enhanced dissolution and anti-BC activities. The taste masking of OC in OC-X is attributed to a unique thermodynamic complexation between OC and xylitol. c-MET, the main molecular target of OC, is a key player in BC development, progression, recurrence, and metastasis. OC is expected to have long-term safety profile at low, food-level doses based on the historical human consumption of olive oil. Other advantages of OC as nutraceutical is its cost-effectiveness based on the sustained plant supply source, relative ease and economic viability of commercial production, and potential for marketing as dietary supplement without the need for full pre-marketing regulatory approval. The use of OC nutraceutical products can be extended not only to prospective BC patients and survivors but also to women with disease risk factors.

Supplementary Material

Refer to Web version on PubMed Central for supplementary material.

ACKNOWLEDGMENTS

The Dafnis family, Corfu Island, Greece, is acknowledged for generously offering the oleocanthal source Governor EVOO. Drs. Seetharama Jois, Turki Al Hagbani, and Mostafa Kamal, University of Louisiana at Monroe, are acknowledged for assistance with some experiments.

Funding

This work was supported by the Louisiana Board of Regents [grant numbers LEQSF (2017-20)-RD-B-07]; the National Cancer Institute of the National Institutes of Health under [grant number R15CA167475].

ABBREVIATIONS:

BC	breast cancer
EVOO	extra-virgin olive oil
OC	oleocanthal
TNBC	triple negative breast cancer
SD	solid dispersion
OC-X	Oleocanthal-(+)-xylitol solid dispersion formulation
PM	physical mixture
SEM	scanning electron microscope
DSC	differential scanning calorimetry
FWHM	full width at half maximum

TGA	thermogravimetric analysis
PXRD	Powder X-ray diffraction
FTIR	Fourier-transform infrared spectroscopy
MS	mass spectrometry
PI	product ion
HPMC	hydroxypropyl methylcellulose
rpm	rotation per minute
E-Tongue	electronic-tongue
DI	discrimination Index
p-c-MET	Phospho-mesenchymal-epithelial transition receptor tyrosine kinase

REFERENCES

Akl MR; Ayoub NM; Mohyeldin MM; Busnena BA; Foudah AI; Liu YY; El Sayed KA Olive Phenolics as c-MET Inhibitors: (−)-Oleocanthal Attenuates Cell Proliferation, Invasiveness, and Tumor Growth in Breast Cancer Models. PLoS One 2014, 9, e97622. [PubMed: 24849787]

Alkhamis KA; Obaidat AA; Nuseirat AF Solid-State Characterization of Fluconazole. Pharm. Dev. Technol 2002, 7, 491–503. [PubMed: 12503530]

Amo K; Arai H; Uebanso T; Fukaya M; Koganei M; Sasaki H; Yamamoto H; Taketani Y; Takeda E Effects of Xylitol on Metabolic Parameters and Visceral Fat Accumulation. J. Clin. Biochem. Nutr 2011, 49, 1–7. [PubMed: 21765599]

Arafa MF; El-Gizawy SA; Osman MA; El Maghraby GM Xylitol as A Potential Co-crystal Co-former for Enhancing Dissolution Rate of Felodipine: Preparation and Evaluation of Sublingual Tablets. Pharm. Dev. Technol 2018, 23, 454–463. [PubMed: 27681386]

Asare-Addo K; Conway BR; Hajamohaideen MJ; Kaialy W; Nokhodchi A; Larhrib H Aqueous and Hydro-alcoholic Media Effects on Polyols. Colloids Surf. B Biointerfaces 2013, 111, 24–29. [PubMed: 23777788]

Ayoub NM; Siddique AB; Ebrahim HY; Mohyeldin MM; El Sayed KA The Olive Oil Phenolic (−)-Oleocanthal Modulates Estrogen Receptor Expression in Luminal Breast Cancer in vitro and in vivo and Synergizes with Tamoxifen Treatment. Eur. J. Pharmacol 2017, 810, 100–111. [PubMed: 28625568]

Baghel S; Cathcart H; O'Reilly NJ Polymeric Amorphous Solid Dispersions: A Review of Amorphization, Crystallization, Stabilization, Solid-State Characterization, and Aqueous Solubilization of Biopharmaceutical Classification System Class II Drugs. J. Pharm. Sci 2016, 105, 2527–2544. [PubMed: 26886314]

Batarseh YS; Mohamed LA; Al Rihani SB; Mousa YM; Siddique AB; El Sayed KA; Kaddoumi A Oleocanthal Ameliorates Amyloid-beta Oligomers' Toxicity on Astrocytes and Neuronal Cells: In vitro studies. Neuroscience 2017, 352, 204–215. [PubMed: 28392295]

Chang Z; Liu D; Yang Z; Wu J; Zhuang W; Niu H; Ying H Efficient Xylitol Production from Cornstalk Hydrolysate using Engineered *Escherichia coli* Whole Cells. J. Agric. Food Chem 2018, 66, 13209–13216. [PubMed: 30465421]

Cicerale S; Breslin PAS; Beauchamp GK; Keast RSJ Sensory Characterization of The Irritant Properties of Oleocanthal, A Natural Anti-inflammatory Agent in Extra-virgin Olive Oils. Chem. Senses, 2009, 34, 333–339. [PubMed: 19273462]

Ciosek P; Wróblewski W Sensor Arrays for Liquid Sensing – Electronic Tongue Systems. Analyst 2007, 132, 963–978. [PubMed: 17893798]

Comen E; Norton L; Massagu EJ Clinical Implications of Cancer Self-Seeding. Nat. Rev. Clin. Oncol 2011, 8, 369–377. [PubMed: 21522121]

Cui J; Yu B; Zhao Y; Zhu W; Li H; Lou H; Zhai G Enhancement of Oral Absorption of Curcumin by Self-Microemulsifying Drug Delivery Systems. Int. J. Pharm 2009, 371, 148–155. [PubMed: 19124065]

Cusimano A; Balasus D; Azzolina A; Augello G; Emma MR; Di Sano C; Gramignoli R; Strom SC; McCubrey JA; Montalto G; Cervello M Oleocanthal Exerts Antitumor Effects on Human Liver and Colon Cancer Cells through ROS Generation. Int. J. Oncol 2017, 51, 533–544. [PubMed: 28656311]

Dyminski SD; Paterno L; Takeda H; Bolini H; H. C. Mattoso L; Cândido L Correlation Between Human Panel and Electronic Tongue Responses on The Analysis of Commercial Sweeteners 2006, 4, 403–408.

Escricha E; Morala R; Solanas M Olive Oil, an Essential Component of The Mediterranean Diet, and Breast Cancer. Public Health Nut 2011, 14, 2323–2332.

Farah da Silva A; Suzuki É; Ferreira A; Gomes Oliveira M; da Silva S; Rezende Barbosa Raposo N In Vitro Inhibition of Adhesion of Escherichia coli Strains by Xylitol. Braz. Arch. Biol. Tech 2011, 54, 235–241.

Fujimoto Y; Hirai N; Takatani-Nakase T; Takahashi K Preparation and Evaluation of Solid Dispersion Tablets by a Simple and Manufacturable Wet Granulation Method Using Porous Calcium Silicate. Chem. Pharm. Bull. (Tokyo) 2016, 64, 311–318. [PubMed: 27039831]

Giusti L; Angeloni C; Barbalace MC; Lacerenza S; Ciregia F; Ronci M; Urbani A; Manera C; Digiacomo M; Macchia M; Mazzoni MR; Lucacchini A; Hrelia S A Proteomic Approach to Uncover Neuroprotective Mechanisms of Oleocanthal against Oxidative Stress. Int. J. Mol. Sci 2018, 19, 2329.

Hagbani TA; Nazzal S Curcumin Complexation with Cyclodextrins by The Autoclave Process: Method Development and Characterization of Complex Formation. Int. J. Pharm 2017, 520, 173–180. [PubMed: 28167265]

Ho-Yen CM; Green AR; Rakha EA; Brentnall AR; Ellis IO; Kermorgant S; Jones JL c-Met in invasive breast cancer. Is There A Relationship with The Basal-Like Subtype? Cancer 2014, 120, 163–171. [PubMed: 24150964]

Ho-Yen CM; Jones JL; Kermorgant S The Clinical and Functional Significance of c-Met in Breast Cancer: A Review. Breast Cancer Res 2015, 17, 52. [PubMed: 25887320]

Jeon WY; Yoon BH; Ko BS; Shim WY; Kim JH Xylitol Production is Increased by Expression of Codon-optimized *Neurospora crassa* Xylose Reductase Gene in *Candida tropicalis.* Bioprocess Biosyst. Eng 2012, 35, 191–198. [PubMed: 21922311]

Kaialy W; Maniruzzaman M; Shojaee S; Nokhodchi A Antisolvent Precipitation of Novel Xylitol-Additive Crystals to Engineer Tablets with Improved Pharmaceutical Performance. Int. J. Pharm 2014, 477, 282–293. [PubMed: 25447824]

Kovalkovičová N, Sutiaková I, Pistl J, Sutiak V. Some Food Toxic for Pets. Interdiscip. Toxicol 2009, 2, 169–176. [PubMed: 21217849]

Kuno Y; Kojima M; Ando S; Nakagami H Evaluation of Rapidly Disintegrating Tablets Manufactured by Phase Transition of Sugar Alcohols. J. Control Release 2005, 105, 16–22. [PubMed: 15955365]

Kobayashi Y; Habara M; Ikezazki H; Chen R; Naito Y; Toko K Advanced Taste Sensors Based on Artificial Lipids with Global Selectivity to Basic Taste Qualities and High Correlation to Sensory Scores. Sensors (Basel, Switzerland) 2010, 10, 3411–3443.

Lee AA; Owyang C Sugars, Sweet Taste Receptors, and Brain Responses. Nutrients 2017, 9, 653.

Legin A; Rudnitskaya A; Lvova L; Vlasov Y; Di Natale C; D'Amico A Evaluation of Italian Wine by The Electric Tongue: Recognition, Quantitative Analysis and Correlation with Human Sensors Perception. Analytica Chimica Acta 2003, 484, 33–44.

Lenhart A; Chey WD A Systematic Review of The Effects of Polyols on Gastrointestinal Health and Irritable Bowel Syndrome. Adv. Nutr 2017, 8, 587–596. [PubMed: 28710145]

Leuner C; Dressman J Improving Drug Solubility for Oral Delivery Using Solid Dispersions. Eur. J. Pharm. Biopharm 2000, 50, 47–60. [PubMed: 10840192]

Madgulkar A; Bandivadekar M; Shid T; Rao S Sugars as Solid Dispersion Carrier to Improve Solubility and Dissolution of The BCS Class II Drug: Clotrimazole. Drug Dev. Ind. Pharm 2016, 42, 28–38. [PubMed: 25874729]

Maniruzzaman M; Morgan DJ; Mendham AP; Pang J; Snowden MJ; Douroumis D Drug-Polymer Intermolecular Interactions in Hot-Melt Extruded Solid Dispersions. Int. J. Pharm 2013, 443, 199–208. [PubMed: 23262428]

Marques M; Löbenberg R; Almukainzi M Simulated Biological Fluids with Possible Application in Dissolution Testing. Dissolution Technol 2011, 18, 15–28.

Medarevic DP; Kachrimanis K; Mitric M; Djuris J; Djuric Z; Ibric S Dissolution Rate Enhancement and Physicochemical Characterization of Carbamazepine-Poloxamer Solid Dispersions. Pharm. Dev. Technol 2016, 21, 268–276. [PubMed: 25582577]

Milgrom P; Ly KA; Rothen M Xylitol and Its Vehicles for Public Health Needs. Adv. Dent. Res 2009, 21, 44–47. [PubMed: 19710081]

Milgrom P; Ly KA; Tut OK; Mancl L; Roberts MC; Briand K; Gancio MJ Xylitol Pediatric Topical Oral Syrup to Prevent Dental Caries: A Double-Blind Randomized Clinical Trial of Efficacy. Arch. Pediatr. Adolesc. Med 2009, 163, 601–607. [PubMed: 19581542]

National Research Council. Guide for the Care and Use of Laboratory Animals; The National Academies Press: Washington, DC, USA, 2011 Available online: http://grants.nih.gov/grants/olaw/Guide-for-the-Careand-Use-of-Laboratory-Animals.pdf.

Pei T; Meng Q; Han J; Sun H; Li L; Song R; Sun B; Pan S; Liang D; Liu L (−)-Oleocanthal Inhibits Growth and Metastasis by Blocking Activation of STAT3 in Human Hepatocellular Carcinoma. Oncotarget 2016, 7, 43475–43491. [PubMed: 27259268]

Peyrot des Gachons C; Uchida K; Bryant B; Shima A; Sperry JB; Dankulich-Nagrudny L; Tominaga M; Smith AB; Beauchamp GK; Breslin PA Unusual Pungency from Extra-virgin Olive Oil is Attributable to Restricted Spatial Expression of The Receptor of oleocanthal. J Neurosci 2011, 31, 999–1009. [PubMed: 21248124]

Pienta KJ; Robertson BA; Coffey DS; Taichman RS The Cancer Diaspora: Metastasis Beyond The Seed and Soil Hypothesis. Clin. Cancer Res 2013, 19, 5849–5855. [PubMed: 24100626]

Podrazka M; Baczynska E; Kundys M; Jelen PS; Nery EW Electronic Tongue-A Tool for All Tastes? Biosensors 2018, 8, 3.

Qosa H; Batarseh YS; Mohyeldin MM; El Sayed KA; Keller JN; Kaddoumi A Oleocanthal Enhances Amyloid-beta Clearance from the Brains of TgSwDI Mice and in Vitro across a Human Blood-Brain Barrier Model. ACS Chem. Neurosci 2015, 6, 1849–1859. [PubMed: 26348065]

Sadler MJ Foods, nutrients and food ingredients with authorised EU health claimsWoodhead Publication: Cambridge, UK; Waltham, MA, 2014, Volume 1.

Samiee S; Berardi P; Bouganim N; Vandermeer L; Arnaout A; Dent S; Mirsky D; Chasen M; Caudrelier JM; Clemons M Excision of The Primary Tumor in Patients with Metastatic Breast Cancer: A Clinical Dilemma. Curr. Oncol 2012, 19, e270–279. [PubMed: 22876156]

Sanchez de Medina V; Miho H; Melliou E; Magiatis P; Priego-Capote F; Luque de Castro MD Quantitative Method for Determination of Oleocanthal and Oleacein in Virgin Olive Oils by Liquid Chromatography-Tandem Mass Spectrometry. Talanta 2017, 162, 24–31. [PubMed: 27837824]

Sareen S; Mathew G; Joseph L Improvement in Solubility of Poor Water-Soluble Drugs by Solid Dispersion. Int. J. Pharm. Investig 2012, 2, 12–17.

Segura-Carretero A; Curiel JA Current Disease-Targets for Oleocanthal as Promising Natural Therapeutic Agent. Int. J. Mol. Sci 2018, 19, 2899.

Shen P; Walker GD; Yuan Y; Reynolds C; Reynolds EC Polyols and Remineralisation of Enamel Subsurface Lesions. J. Dent 2017, 66, 71–75. [PubMed: 28838679]

Siddique A; Ayoub NM; Tajmim A; Meyer SA; Hill RA; El Sayed KA (−)-Oleocanthal prevents breast cancer locoregional recurrence after primary tumor surgical excision and neoadjuvant targeted therapy in orthotopic nude mouse models. Cancers (Basel) 2019`a`, 11, 637.

Siddique A; Ibrahim HY; Akl MR; Ayoub NM; Goda AA; Mohyeldin MM; Nagumalli SK; Hananeh WM; Liu YY; Meyer SA; El Sayed KA (−)-Oleocanthal Combined with Lapatinib Treatment Synergized against HER-2 Positive Breast Cancer in vitro and in vivo. Nutrients 2019`b`, 11, 412.

Siddique A; Ebrahim HE; Qusa M; Btarsah Y; Fayaad A; Tajmim A; Nazzal S; Kaddoumi A; El Sayed KA Novel Liquid-Liquid Extraction and Self-Emulsion Methods for Simplified Isolation of Extra-virgin Olive Oil Phenolics with Emphasis on (−)-Oleocanthal and Its Oral Anti-Breast Cancer Activity. PLoS ONE 2019`c`, 14, e0214798. [PubMed: 30964898]

Tamura M; Hoshi C; Hori S Xylitol Affects The Intestinal Microbiota and Metabolism of Daidzein in Adult Male Mice. Int. J. Mol. Sci 2013, 14, 23993–24007. [PubMed: 24336061]

Toledo E; Salas-Salvado J; Donat-Vargas C; Buil-Cosiales P; Estruch R; Ros E; Corella D; Fitó M; Hu FB; Arós F; Gómez-Gracia E; Romaguera D; Ortega-Calvo M; Serra-Majem L; Pintó X; Schröder H; Basora J; Sorlí JV; Bulló M; Serra-Mir M; Martinez-Gonzalez MA Mediterranean Diet and Invasive Breast Cancer Risk Among Women at High Cardiovascular Risk in The PREDIMED Trial: A Randomized Clinical Trial. JAMA Internal. Medicine, 2015, 175, 1752–1760. [PubMed: 26365989]

Tran PH; Tran TT; Park JB; Lee BJ Controlled Release Systems Containing Solid Dispersions: Strategies and Mechanisms. Pharm. Res 2011, 28, 2353–2378. [PubMed: 21553168]

Uebanso T; Kano S; Yoshimoto A; Naito C; Shimohata T; Mawatari K; Takahashi A Effects of Consuming Xylitol on Gut Microbiota and Lipid Metabolism in Mice. Nutrients 2017, 9, 756.

Vasconcelos T; Sarmento B; Costa P Solid Dispersions as A Strategy to Improve Oral Bioavailability of Poor Water Soluble Drugs. Drug Discov. Today 2007, 12, 1068–1075. [PubMed: 18061887]

Wei Y; Nedley MP; Bhaduri SB; Bredzinski X; Boddu SHS Masking The Bitter Taste of Injectable Lidocaine HCl Formulation for Dental Procedures. AAPS PharmSciTech 2015, 16, 455–465. [PubMed: 25361901]

Woertz K; Tissen C; Kleinebudde P; Breitkreutz J Taste sensing systems (electronic tongues) for pharmaceutical applications. Int. J. Pharm 2011, 417, 256–271. [PubMed: 21094230]

Zhang X; Zhang Y; Meng Q; Li N; Ren L Evaluation of beef by electronic tongue system TS-5000Z: Flavor Assessment, Recognition and Chemical Compositions According to Its Correlation with Flavor. PloS One 2015, 10, e0137807. [PubMed: 26368555]

Zhang X; Xing H; Zhao Y; Ma Z Pharmaceutical Dispersion Techniques for Dissolution and Bioavailability Enhancement of Poorly Water-Soluble Drugs. Pharmaceutics 2018, 10, 74.

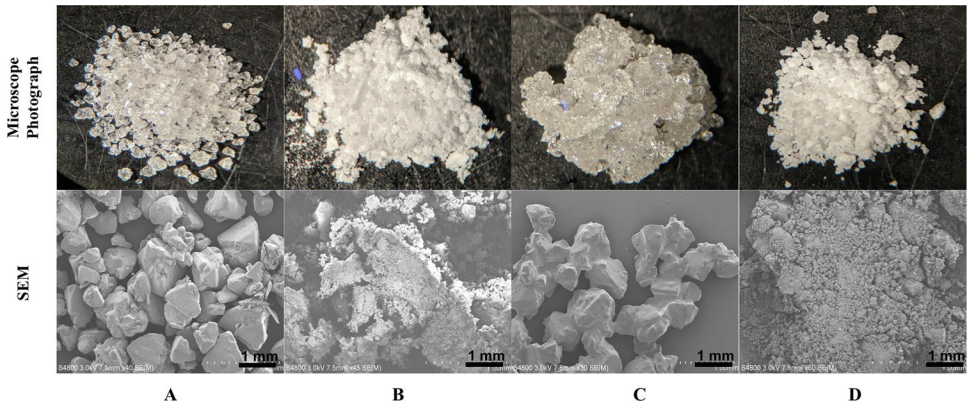

Figure 1.

Upper row: Microscope photographs, magnification 10x. Lower row: Scanning electron microscopy (SEM) of: (A) (+)-Xylitol, (B) Crystallized (+)-xylitol, (C) Physical mixture (PM), (D) OC-X 1:7 SD formulation. The SEM scale bar represents 1 mm. The magnification of A-D is: 40x, 45x, 30x, and 50x *1000, respectively.

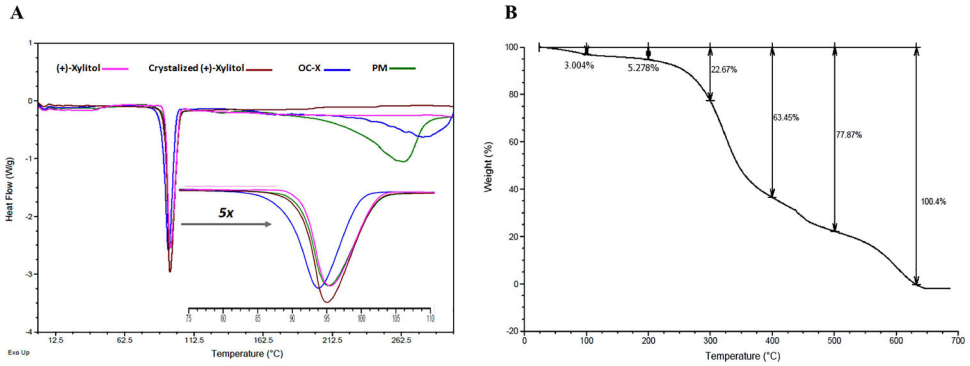

Figure 2.

(A) MTDSC thermograms of (+)-xylitol, crystallized (+)-xylitol, PM, OC-X SD showing OC decomposition started at ~250 °C, with enlargement of (+)-xylitol melting peak at 5X, distinguishing the differences in melting peaks and enthalpy energy of all samples. All runs obtained at a 5 °C min^{-1} heating rate. (B) Thermogravimetric analysis (TGA) of plain, non-formulated OC.

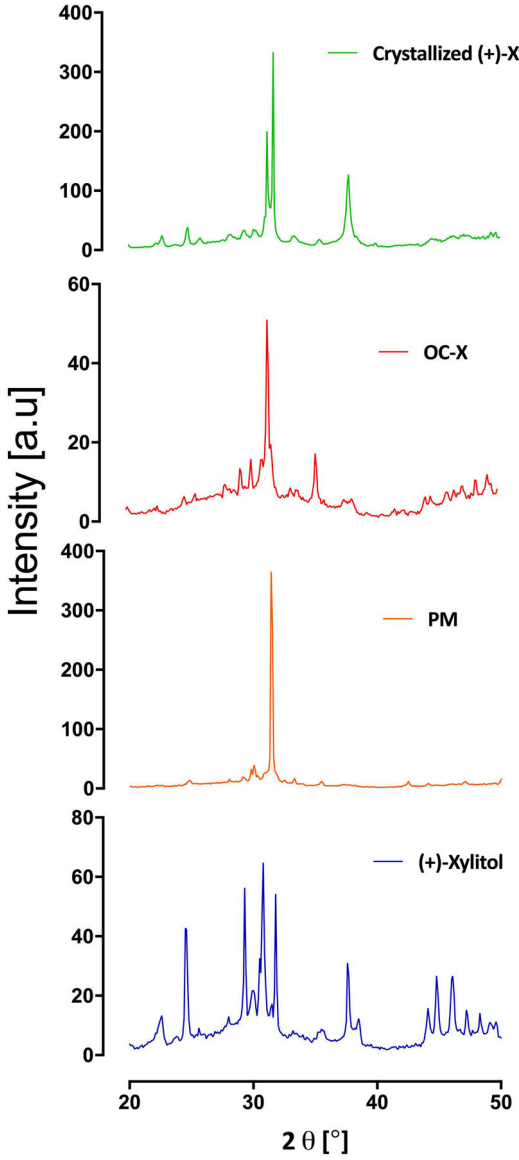

Figure 3.

Powder X-ray diffraction (PXRD) patterns demonstrating crystallite structural evolution of xylitol. From bottom to top: (+)-xylitol, PM, OC-X 1:7 SD, crystalized (+)-xylitol.

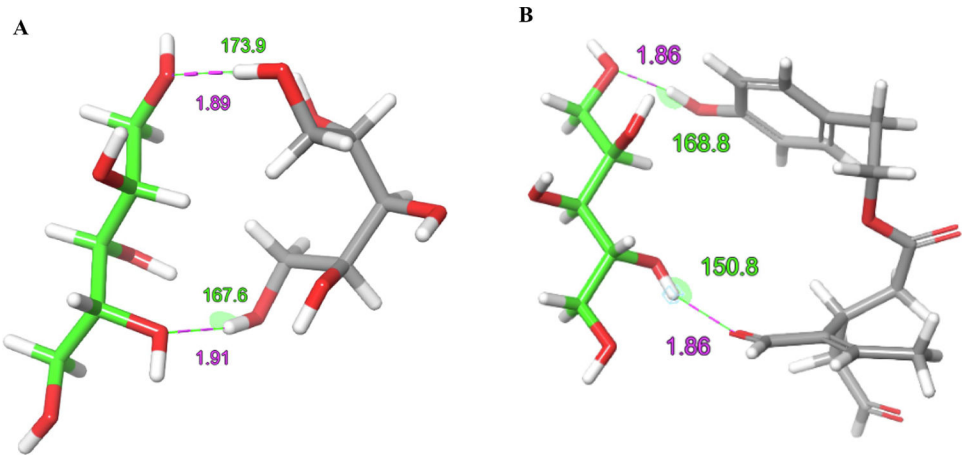

Figure 4.

Molecular modeling of xylitol-xylitol hydrogen bonding interactions (A) and xylitol-OC hydrogen bonding interactions (B) in molecular dynamic, solvent-free mode. Hydrogen bond interactions observed represent those between two xylitol molecules in their crystal structure and the hypothetical interactions between one xylitol molecule and OC in the OC-X SD formulation. Purple line for the thru-space molecular distance in Å between hydrogen bond interacting functional groups. Green line shows the hydrogen bond interactions angle in degrees "°".

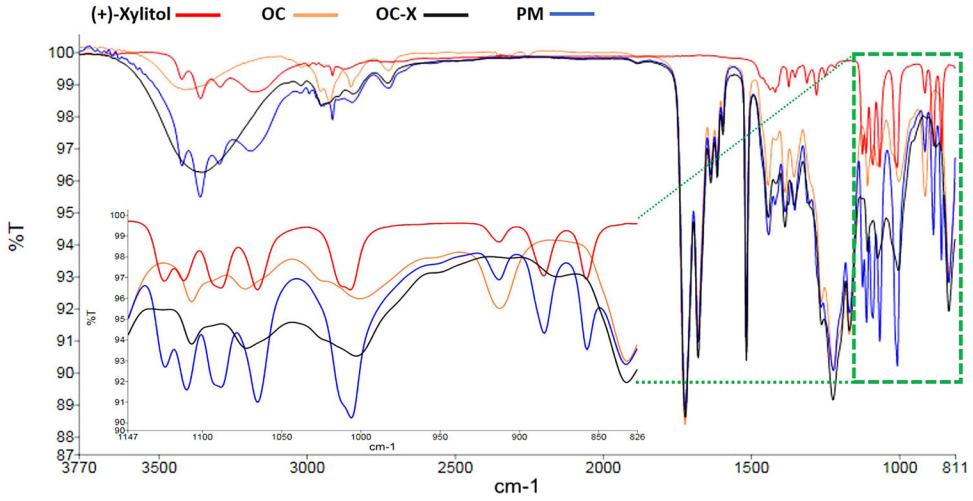

Figure 5.

Fourier-transform infrared (FTIR) spectra of (+)-xylitol (red), plain, non-formulated OC (orange), OC-X 1:7 SD (black), PM (blue), and the zooming expansion of the four samples fingerprint region (825–1147 cm^{-1}).

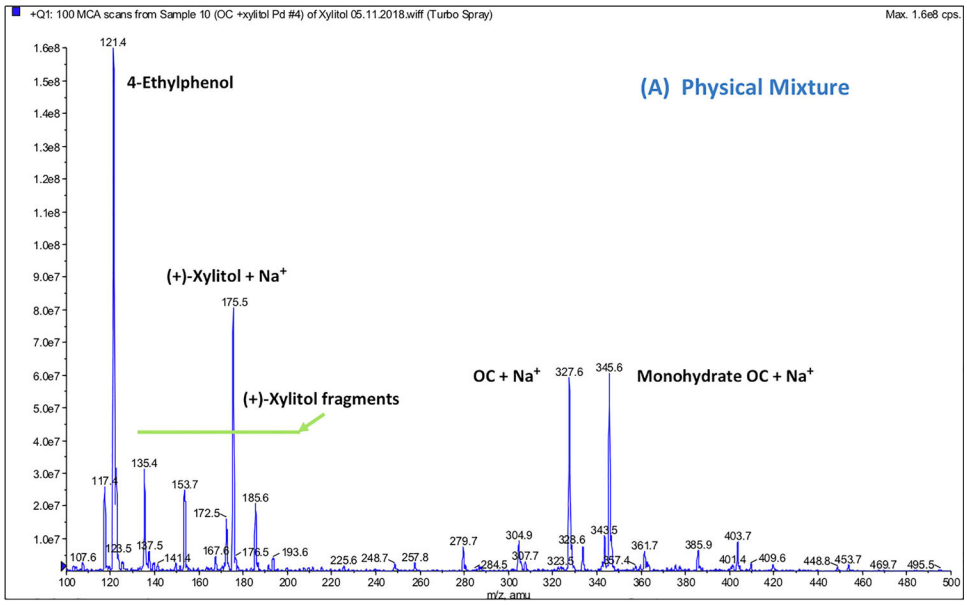

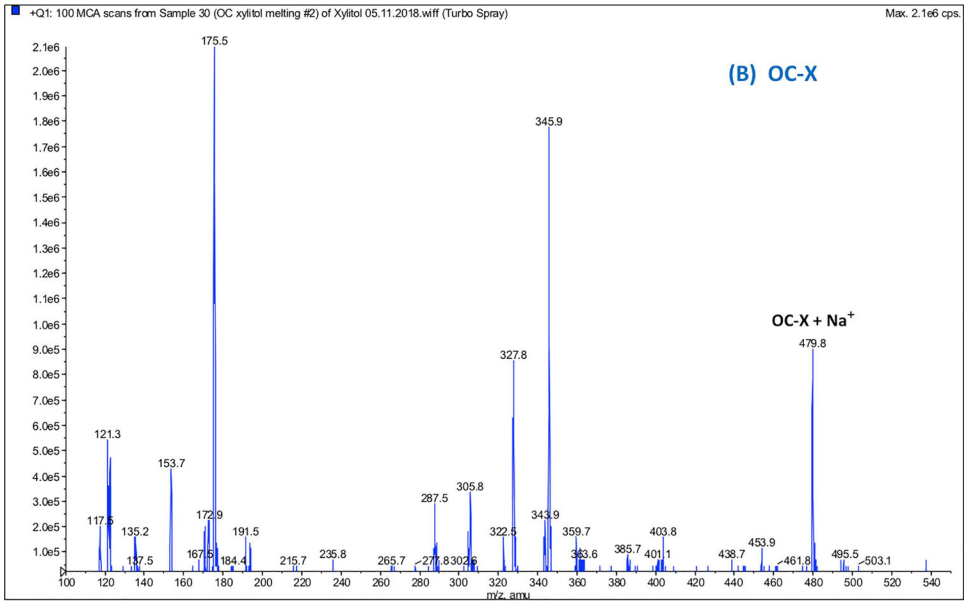

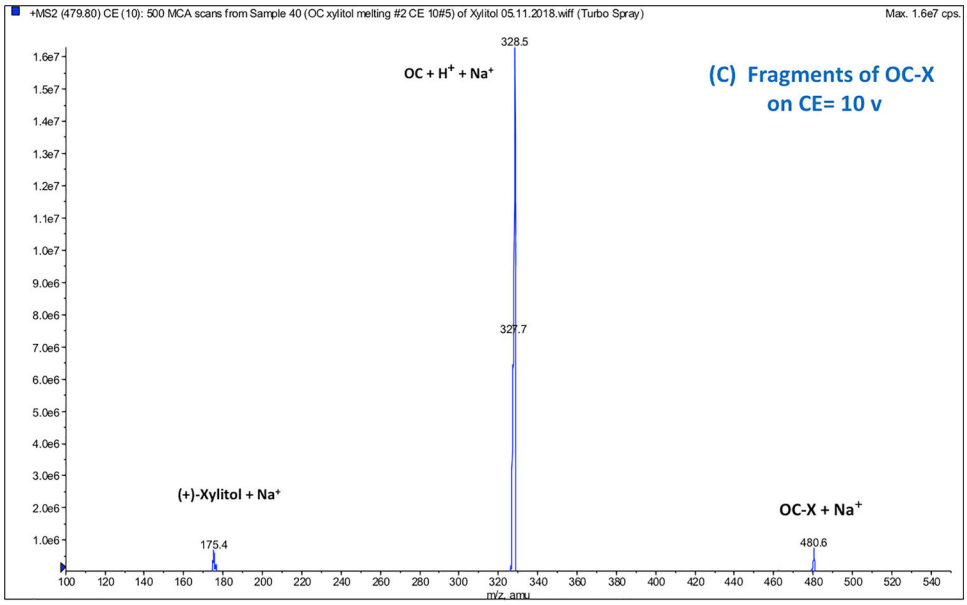

Figure 6.

Full scan Q1 mass spectra of: (A) PM showing ion peaks for individual OC and xylitol, (B) OC-X 1:7 SD showing the molecular ion peak of the OC-xylitol complex Na adduct at *m*/*z* 479.8, (C) ESI-MS-MS Q2 fragmentation product ions of the OC-xylitol complex Na adduct at *m*/*z* 480.6 to individual OC and xylitol Na adducts at collision energy 10V.

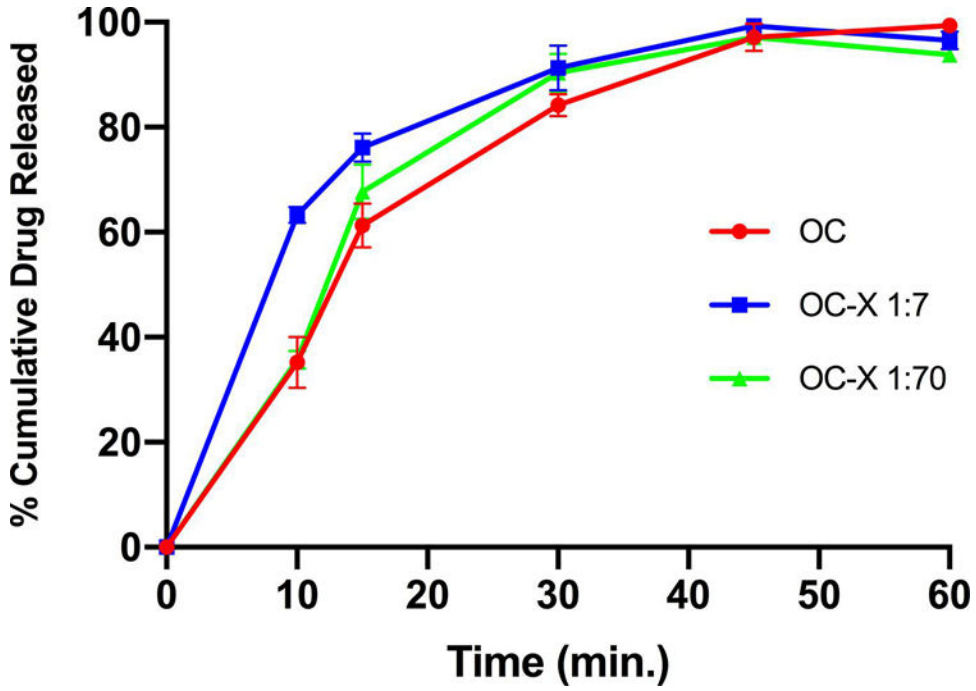

Figure 7.

Comparison of the dissolution profiles of plain non-formulated OC, OC-X 1:7, and OC-X 1:70 SD formulations in artificial saliva, pH 6.8, at 37 °C.

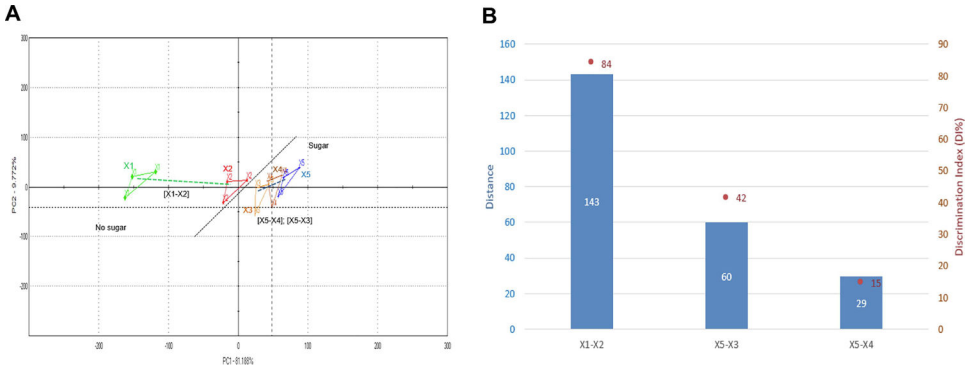

Figure 8.

Electronic-tongue taste comparison assessments. (A) Taste map based on principal component analysis (PCA) of samples; artificial saliva (pH 6.8, X1), plain, non-formulated OC (X2), OC-X 1:7 SD (X3), OC-X 1:70 SD (X4), and (+)-xylitol (X5). (B) The Euclidian distances and Discrimination Index (DI in %) between X1-X5.

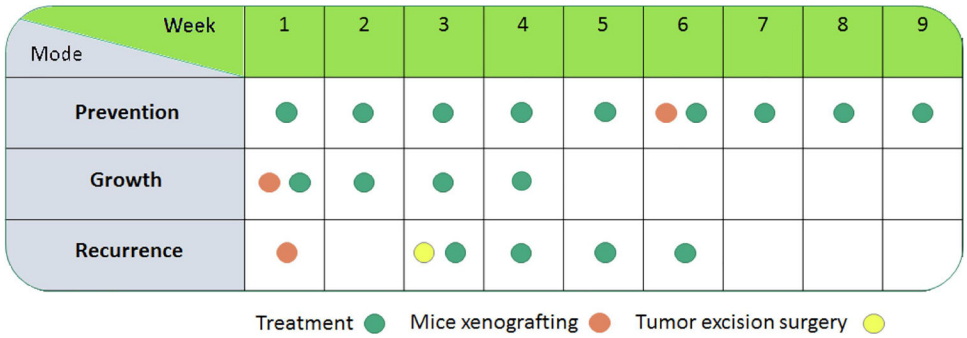

Figure 9.

Overview of OC-X 1:7 SD *in vivo* anti-BC activities. Activities include BC development, growth, and recurrence inhibition.

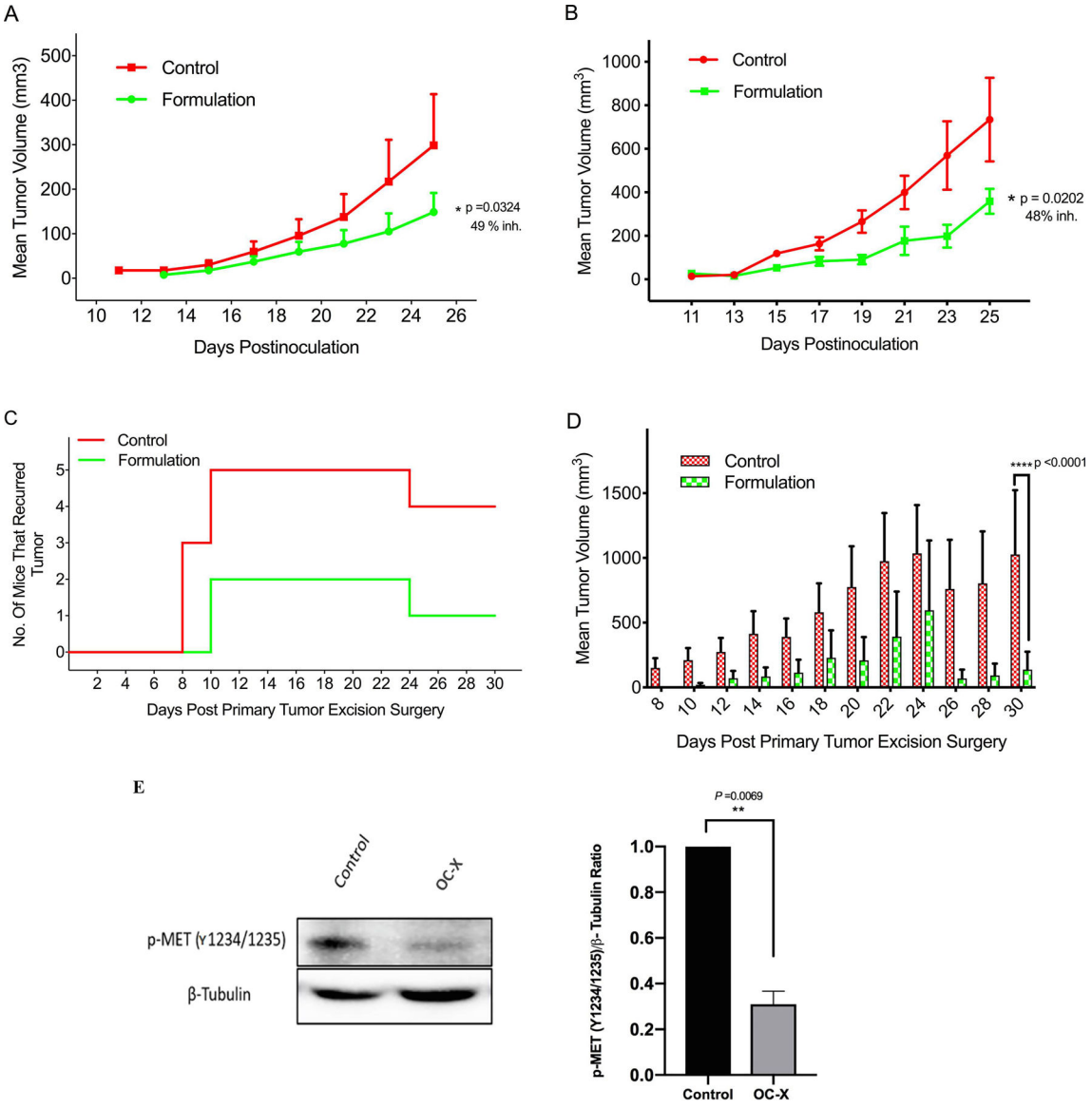

Figure 10.

Anti-TNBC activities of oral 10 mg/kg OC-X 1:7 SD (of OC) in orthotopic athymic nude mice xenograft models. (A) OC-X was used in preventive mode 45 days before tumor cells inoculation and continued for additional 25 days after xenografting. OC-X inhibited 49% of tumor development and growth compared to placebo control, n=5, at the study end. (B) OC-X was used in growth suppression mode, orally used 5 days after tumor cells xenografting and treatment continued for 15 days. OC-X inhibited 48% of tumor growth compared to placebo control, n=4, at the study end. (C) The TNBC MDA-MB-231 cells xenografted into each nude mouse second mammary fat pad. Fifteen days after xenografting, each mouse primary tumor, volume averaged ~400 mm^3, was surgically excised. The next day after the surgery, mice randomized to two groups, n=5, placebo control and OC-X 1:7 SD treated group. Treatment started and continued for additional 30 days. All 5 placebo control mice developed locoregional recurrence tumors while only 2 out of 5 mice treated with OC-X 1:7

SD developed locoregional recurrence tumors (60% recurrence prevention). (D) Comparison of the effects of OC-X and its placebo treatments on recurrence tumor volume over the experiment course. Results expressed as the mean S.E.M. The percentage of tumor volume inhibition values (Inh.) was measured on the final day of the study for the drug-treated mice compared with the control mice. * $p < 0.05$, ** $p < 0.01$, and *** $p < 0.001$ versus placebo control group, using Student's t test. (E) OC-X 1:7 SD significantly reduced the activated c-MET (Y1234/1235) level in collected growth inhibition mode experiment tumors compared to the placebo control group. Right panel is densitometric semi-quantitative analysis for p-c-MET (Y1234/1235)/β tubulin.

Table 1.

Melting peak, onset and end set point, FWHM, ΔH of the samples used in MTDSC.

Samples	Melting peak (°C)	Melting on-set (°C)	Melting end set (°C)	FWHM	ΔH (J g^{-1})
(+)-Xylitol	95.65	92.16	105.24	6.5	196.5
Crystalized (+)-xylitol	95.25	91.91	105.11	6.6	225.8
OC-X SD	94.11	89.53	103.43	6.9	211.7
PM	95.46	91.9	105.13	6.6	187.3